

Article

Influence of Preaging Treatment on Bake-Hardening Response and Electrochemical Corrosion Behavior of High Strength Al-Zn-Mg-Cu-Zr Alloy

Hui Li ^{1,2,*} , Xiao-Teng Liu ^{2,3} and Jia-Yi Wang ^{1,2}

¹ College of Engineering, Yantai Nanshan University, Yantai 265700, China

² National Engineering Research Center for Plastic Working of Aluminum Alloys, Shandong Nanshan aluminum Co Ltd., Yantai 265700, China

³ Testing Center, Hang Xin Material Technology Co. Ltd., Yantai 265700, China

* Correspondence: lihui9@nanshan.edu.cn; Tel.: +86-0535-8609-592

Received: 24 July 2019; Accepted: 13 August 2019; Published: 15 August 2019



Abstract: The influence of preaging (PA) treatments on the bake hardening (BH) response of a AlZnMgCuZr aluminum alloy which served as automotive body structures were studied in this paper. A novel two-step PA treatment was particularly designed and further employed. The mechanical properties of the alloy were tested in detail. The microstructure was characterized by optical microscope (OM), transmission electron microscopy (TEM) and 3D measuring laser microscope (3D-MLM). Meanwhile, the corrosion behavior was investigated by electrochemical impedance spectroscopy (EIS) and potentiodynamic polarization. The results indicated that the PA treatment was beneficial for the improvement of BH response after baking at 180 °C immediately after the solution treatment and the micro-hardness reached the peak value (194 HV) after 10 h holding, which had a percentage improvement of 110.87% compared to the hardness under the solution condition. The PA treatments decreased natural aging (NA) adverse effects, while it had the lowest NA effect and optimal BH response under 120 °C/20 min. Such a novel two-step PA treatment was revealed further to decrease the NA effect and increase the BH response compared to the optimal PA treatment, in particular, the BH value could reach 168 MPa and was 21.7% higher than that of optimal PA + NA treatment. The optimal corrosion resistance has been shown up by the combined characterizations of potentiodynamic polarization curves, EIS Nyquist plots, and 3D-MLM images.

Keywords: Al-Zn-Mg-Cu-Zr aluminum alloy; bake hardening response; two-step preaging treatment; electrochemical corrosion behavior

1. Introduction

Lightweight has become an important direction for the development of automobiles [1]. The path to lightweight development is mainly divided into two aspects from the perspective of materials: Substitution of light material for conventional steel [2–4], such as 6000 series aluminum alloy, which has low density and a combination of strength and plasticity; and application of advanced high-strength steels [5,6], such as DP steel, TRIP steel and Q&P steel. In regards to aluminum for lightweight automotive development, previous studies were mainly focused on the research of 6000 series aluminum for panels, such as the subduction of detrimental natural aging (NA) effect and the enhancement of bake hardening (BH) response [7,8]. However, they are not competitive with respect to current high strength steels for structural components.

In contrast, 7000 series high strength aluminum alloy, which has higher specific strength compared to advanced high strength steels, has great application potential in lightweight body structures.

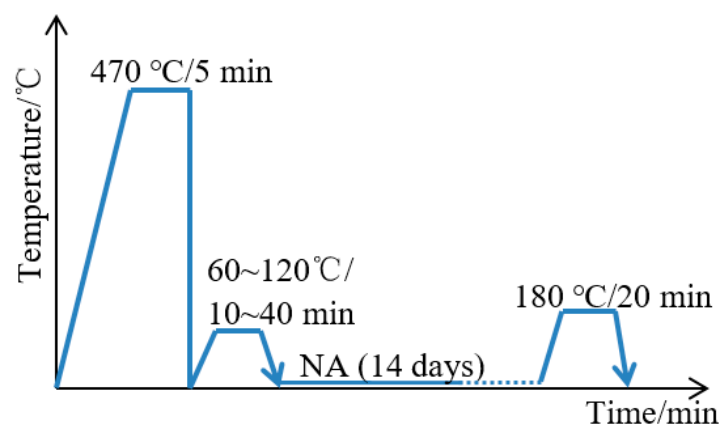
However, its low formability requires multi-step forming processes with intermediate heat treatments. Previous research on 7000 series aluminum were based on its application in the aerospace field, comprising the influence of homogenization treatment on crystallization phases [9,10] and the precipitation behavior of hardening phases, as well as its influence on properties during artificial aging (AA) treatment [11,12] and multistage artificial aging treatment (RRA) [13,14]. It was found that the maximum aging strength was achieved under 120 °C/24 h or 180 °C/12 h, which is not suitable for production of auto sheet. However, studies on the manufacturing and application properties for automotive body structures are very rare. Recently, a number of studies were attempted on the warm forming process to improve formability. Kumar and Ross [15] investigated the warm forming process of a AlZnMg alloy and found that T4 temper had the best combination of warm formability and high post-paint baking strength. Huo et al. [16] found that the peak-aged 7075 alloy exhibited enhanced formability and maintained high post-forming strength under the appropriate temperature of 200 °C, but the warm process would change the microstructure and further decrease the strength. Furthermore, some other studies investigated the influence of heat treatment on BH response. Cao et al. [17] found that preaging (PA) treatment improved the age hardening response and precipitation behavior of a novel Al–5.2Mg–0.45Cu–2.0Zn alloy. Lee et al. [18] studied the effect of PA treatment on BH response of 7075 aluminum alloy from the angle of the precipitation phase and confirmed the effectiveness of PA. However, the optimization of heat treatment to eliminate the NA effect and improve BH response is dramatically demanded, and its influence on corrosion resistance is also needed in order to study more extensive applications of 7000 series aluminum in automotive body structures.

In our present study, an Al–Zn–Mg–Cu–Zr 7000 series plate was systematically investigated based on the application requirement of automotive body structures, including the influence of PA treatment on NA adverse effect, BH response, and other related properties. A novel two-step PA treatment that was properly aimed at changing the occurrence state of alloying elements and improving the BH response, was especially designed. The corrosion behavior was fully characterized by potentiodynamic polarization curves, electrochemical impedance spectroscopy (EIS), Nyquist plots and 3D measuring laser microscope (3D–MLM) images.

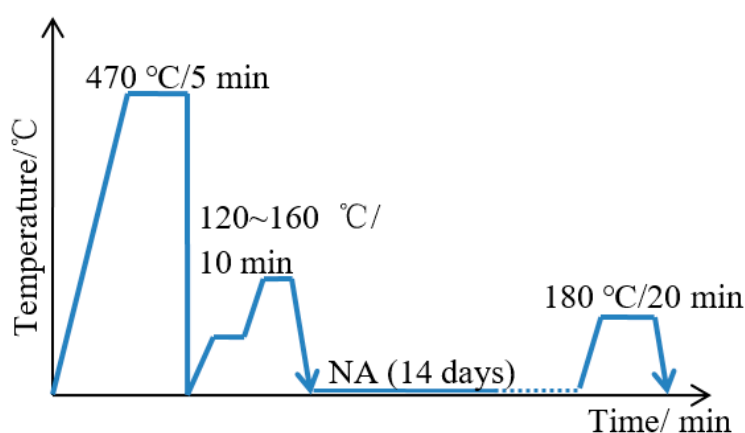
2. Materials and Experimental Methods

2.1. Materials and Heat Treatment

The Al–5.36Zn–2.42Mg–1.78Cu–0.12Zr–0.15Fe (wt%) 7000 series aluminum alloy was used in this experiment. The heat treatments were performed using a salt bath furnace (Huadong Furnace Co., Jiangsu, China). The casting slab was homogenized at 460 °C for 24 h to eliminate the ingot defects such as coarse grains and sharpened phases, and then hot and cold rolled to a final thickness of 1.2 mm. The solution treatments were performed at 470 °C for 5 min and then water cooled to room temperature. The following heat treatments were carried out in a chamber electric furnace immediately: (1) AA at 180 °C for 1, 2, 4, 6, 8, 10, 24, 48, 60 and 72 h; (2) PA at 60, 90 and 120 °C for 10, 20 and 40 min respectively, then storage at room temperature for 14 days, and finally baked at 180 °C for 20 min (as shown in Figure 1a); (3) novel two-step PA treatment, first PA at 120 °C for 10 min, and then holding at 160 °C for 10 min (as shown in Figure 1b).



(a)



(b)

Figure 1. Schematic diagram of heat treatment (a) preaging (PA) treatment; (b) novel two-step PA treatment.

2.2. Mechanical Testing

The uniaxial tensile tests were carried out on a CMT5105 multifunctional tensile testing machine (SANS Testing Machine Co., Shenzhen, China) using a displacement rate of 0.25 mm min^{-1} based on GB/T228.1–2010. The A25 sample gauge length was used. A minimum of three tests were performed for each condition. Real time hardness tests after different heat treatments were carried on a HV–1000 tester (Haoxinda Ltd Co., Shenzhen, China) with 500 g force and 10 s dwell time. Nine indentations were performed and evaluated and the average value was obtained after removal of the maximum and minimum ones.

2.3. Electrochemical Measurement

The electrochemical measurements were carried out in a three electrode cell system using a RST5100 electrochemical workstation (Centome Ltd Co., Chengdu, China). The specimens after different heat treatments were designed for working electrodes and immersed in 3.4 wt% NaCl aqueous solution at room temperature. The Pt foil and saturated calomel electrode were utilized as the counter electrode and reference electrode, respectively.

Both the potentiodynamic polarization curves and EIS were conducted to investigate the corrosion behavior. The open circuit potential reached stable after immersion for 1200 s, and the EIS measurement was performed under the frequency range of 100 kHz to 0.01 Hz and sinusoidal voltage amplitude

of 5 mV. Then, the potentiodynamic polarization measurements proceeded in the voltage range of $-0.9\sim 0.6$ V.

2.4. Microstructure Investigation

The characterization of metallurgical microstructure was performed with an Axio Imager M2m Zeiss microscope (Zeiss Co., Oberkochen, Germany). The specimens were etched for 60 s in HBF_4 (4 mL) + H_2O (200 mL) solution. Transmission electron microscopy (TEM, JEM-2010F, Hillsboro, OR, USA) measurements were carried out at an acceleration voltage of 200 kV. The selected area electron diffraction (SAED) technique was used to characterize the precipitation phase. The specimens were mechanically grounded to 40 μm thickness and punched out into a diameter of 3 mm, and then etched by double-jet polishing using a solution of 1000 mL methanol and 500 mL HNO_3 at 12 V voltage and 243 K temperature. The three dimensional height map of the corroded surface was characterized using an Olympus OLS4100 3D-MLM (Olympus Co., Tokyo, Japan) with semiconductor laser.

3. Results and Discussions

3.1. Metallurgical Microstructure

Figure 2 gives the metallurgical microstructures of the experimental aluminum alloy under different conditions. Compared to the as-cast structure, the grain sizes became fine and the coarse sharpened AlZnMgCu quaternary crystallization phases became rounded after homogenization treatment. After being hot rolled, the microstructure had elongated band tissue because of the low finishing rolling temperature, which reduced the recrystallization behavior. The grains changed into equiaxial based on the recrystallization mechanism during the solution treatment, and had an average size value of 15 μm .

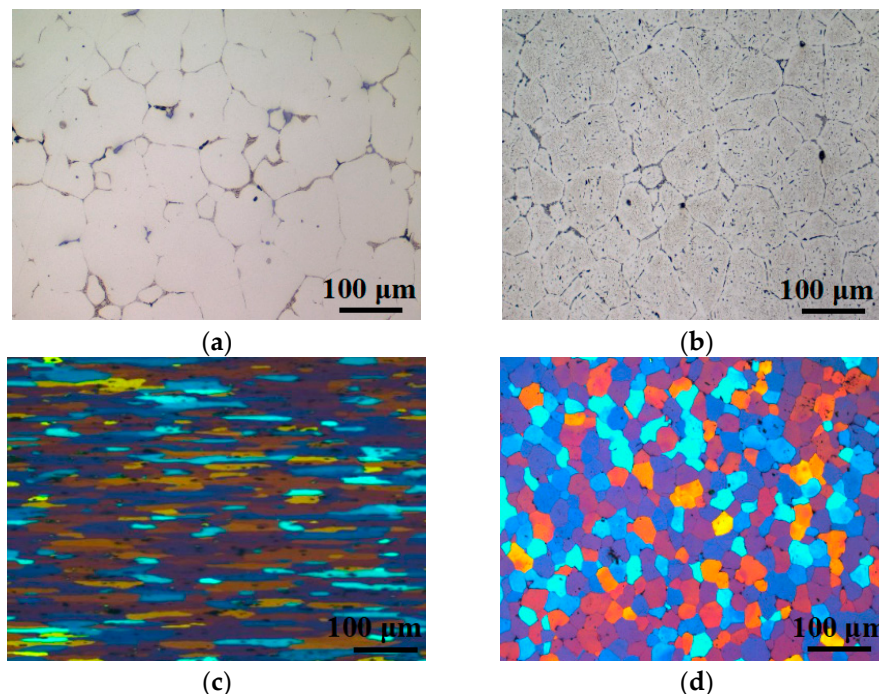
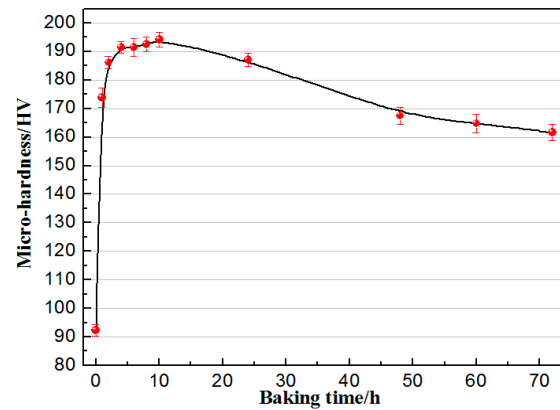


Figure 2. Metallurgical microstructure under different conditions: (a) As-cast; (b) homogenization; (c) hot rolled; (d) solution treatment.

3.2. BH Response at 180 °C after Solution Treatment

Figure 3 presents the evolution behavior of micro-hardness and TEM fine microstructure after holding at 180 °C for different times. With the increasing of holding time, the micro-hardness

increased sharply first and reached the peak value (194 HV) after 10 h holding, which was a percentage improvement of 110.87% compared to the hardness (92 HV) under solution condition, then it had a decreasing trend and tended to become steady after 60 h.



(a)

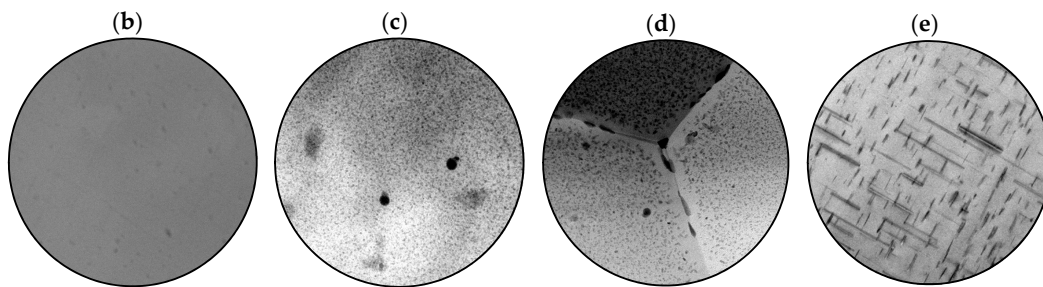


Figure 3. Micro-hardness and microstructure after baking at 180 °C for different times (a) micro-hardness evolution; (b) TEM graphs at point b; (c) point c; (d) point d; (e) point e.

The TEM graphs show the microcosmic change during the bake process. The precipitation process of experimental aluminum was as follows:

SSSS (supersaturated solid solution) → GP zones (Guinier Preston) → η' → η (MgZn_2).

The sample was under aged after 1 h holding, and a large number of nano η' hardening phases were precipitated in the matrix. η' phase was the main strengthening phase of the under aged samples, which was coherent with the matrix, and had an orientation relationship of $(001)_{\eta'} \parallel \{111\}_{\text{Al}}$; $[\bar{1}1\bar{2}0]_{\eta'} \parallel \langle 111 \rangle_{\text{Al}}$; $(10\bar{1}0)_{\eta'} \parallel \{110\}_{\text{Al}}$ [19,20]. There exists different viewpoints of the formation and evolution of η' phase. Mondolfo et al. [21] think that η' phase was formed at the stacking fault of solution samples, while Graf [22] believes that it could be precipitated directly. The precipitation-free zone (PFZ) with 40~70 nm width was observed near the grain boundary after holding for 10 h and the grain boundary was decorated with 50~80 nm precipitation phase. The specimen was over aged after 60 h holding, when the lath-type and rod-like η phases existed in the grain, which were incoherent with the matrix and decreased the hardness [23].

3.3. Influence of PA on Hardness and Microstructures

The influence of PA treatment on adverse NA effect is shown in Figure 4. PA time and temperature have great effect on micro-hardness evolution during the NA process. After the given PA treatment under different temperatures for different times, the micro-hardness increased for all specimens during the NA process, with the difference lying in the increments. The specimen after PA under 90 °C/10 min had the maximum NA increment, which reached 23 HV, while the one after 120 °C/20 min had the minimum increment of 14 HV, which was considered as the optimal PA process.

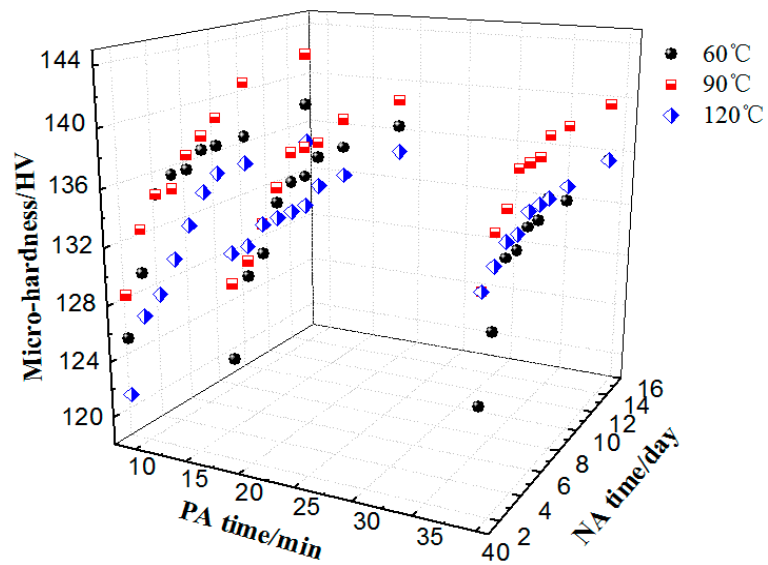


Figure 4. Influence of PA temperature and time on natural aging (NA) effect.

Figure 5 shows the TEM graphs and corresponding SAED of NA, NA + BH, optimal PA + NA, and PA + NA + BH. It can be seen that the size, morphology and quantity of precipitates were different. The main strengthening phases were the GP zones before BH treatment, whereas η' were the dominant hardening phases after BH treatment.

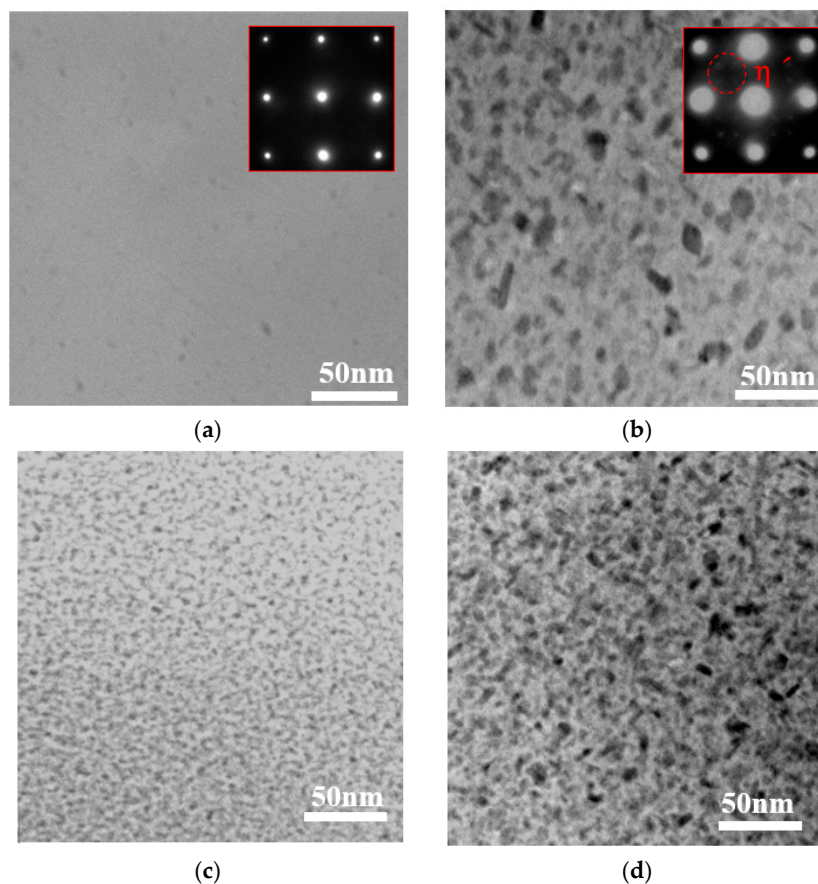


Figure 5. TEM graphs after different treatments: (a) NA; (b) NA +bake hardening (BH); (c) PA + NA; (d) PA + NA + BH.

3.4. Novel Two-Step PA Treatment and Influence on Properties

The evolution behavior of mechanical properties after different heat treatments are shown in Figure 6. The strength of the sample without PA treatment was decreased after bake treatment, and the yield strength and tension strength had a decreasing value of 40 MPa and 67 MPa, respectively. PA treatment increased the BH response, especially the two-step PA treatment, which had a BH value of 168 MPa and was 21.7% higher than that of optimal PA treatment. However, the elongation of the two-step sample was slightly lower than PA.

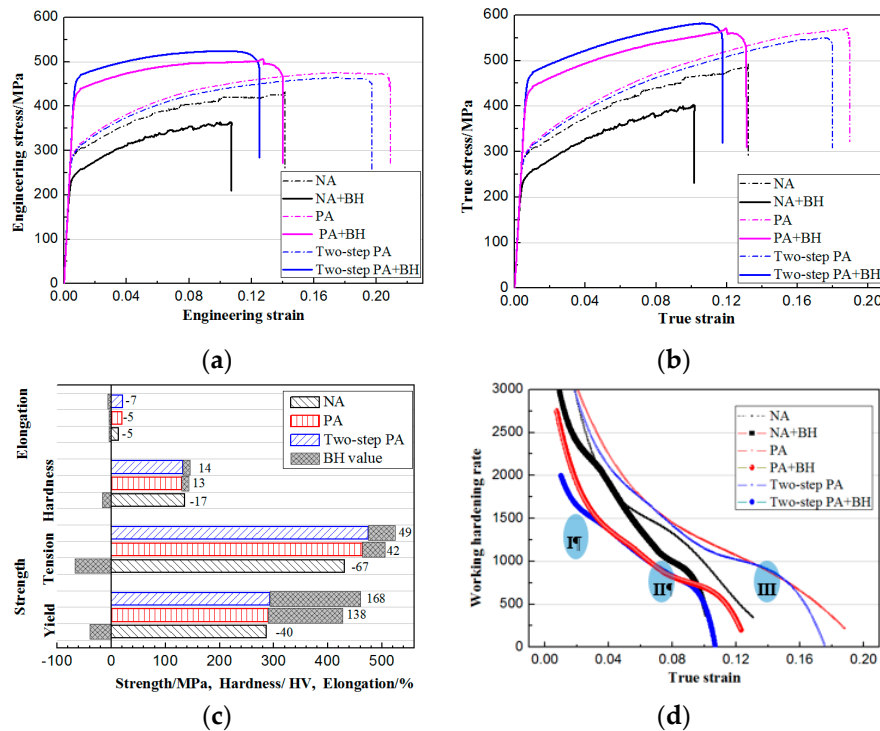


Figure 6. Tension properties after different heat treatment (a) engineering strain-stress curve; (b) true strain-stress curve; (c) change of properties after BH; (d) work hardening rate.

The true stresses of the experimental aluminum alloy varied almost linearly with the true strain during the plastic deformation stage. Through differential of true strain, the work hardening rate was obtained.

$$\Theta = \frac{d\sigma}{d\varepsilon} \tag{1}$$

where Θ is the work hardening rate, σ is true stress, ε is true strain.

The evolution of the work hardening rate with true strain had three stages for all the specimens: (1) Stage I, in which the hardening rate decreased sharply with strain because of the low dislocation density and their weak interaction; (2) stage II, in which the work hardening rate decreased slowly due to the increase of boundaries and dislocation multiplication; (3) stage III, the formation rate of dislocations were very slow and the hardening rate decreased sharply until cracking.

In order to characterize the strain hardening exponent explicitly, the modified Crussard–Jaoul (C–J) equation, based on the Swift equation [24] was used.

$$\ln\left(\frac{d\sigma}{d\varepsilon}\right) = (1 - n_{Swift}) \ln \sigma - \ln(Cn_{Swift}) \tag{2}$$

where σ is true stress; ε is true strain; C is material constant; n_{Swift} is the strain hardening exponent and the smaller the n_{Swift} value is, the higher the hardening ability.

Through calculation of $\ln(d\sigma/d\varepsilon)$ and $\ln\sigma$, the modified C–J curves were obtained as shown in Figure 7. The slopes of the curves represent the value of $1-n_{\text{Swift}}$, and the n_{Swift} and ε_t are gathered in Table 1. $n_{\text{Swift}1}$, $n_{\text{Swift}2}$ and $n_{\text{Swift}3}$ are strain hardening exponents at different deformation stages, and $\varepsilon_{\text{tr}1}$ and $\varepsilon_{\text{tr}2}$ are strain of the turning point of the slope.

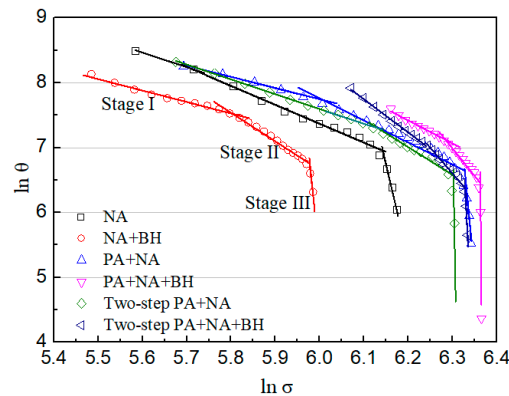


Figure 7. Crussard–Jaoul (C–J) curve of different heat treatments.

Table 1. C–J parameters of different heat treatments.

| Heat Treatment | Stage | Stage I | | Stage II | | Stage III |
|------------------|-------|---------------------|----------------------------|---------------------|----------------------------|---------------------|
| | | $n_{\text{Swift}1}$ | $\varepsilon_{\text{tr}1}$ | $n_{\text{Swift}2}$ | $\varepsilon_{\text{tr}2}$ | $n_{\text{Swift}3}$ |
| NA | | 3.239 | 0.01189 | 3.912 | 0.09691 | 29.303 |
| NA + BH | | 2.756 | 0.04187 | 5.412 | 0.09049 | 62.158 |
| PA | | 2.744 | 0.04038 | 4.409 | 0.15059 | 63.115 |
| PA + BH | | 6.108 | 0.06277 | 8.877 | 0.10948 | 150.413 |
| Two-step PA | | 3.285 | 0.07753 | 5.276 | 0.15436 | 370.775 |
| Two-step PA + BH | | 4.566 | 0.04899 | 9.464 | 0.0958 | 777.251 |

Compared to the characterization of work hardening behavior shown in Figure 6d, the combination of Figure 7 and Table 1 could represent the strain hardening exponent more explicitly under different deformation stages. During Stage I, the $n_{\text{Swift}1}$ value ranged from 2.75 to 6.11 and the $\varepsilon_{\text{tr}1}$ value had a range of 0.011~0.078 for the specimens after different heat treatments. For specimens after PA + NA treatment, the bake process reduced the strain hardening ability. The $n_{\text{Swift}2}$ value of stage II had a range of 3.91~9.47, which represents the decreasing of hardening ability quantitatively. For the specimens after PA+BH and two-step PA + BH treatments, stage III arrived, during which the hardening exponent decreased sharply, while the $\varepsilon_{\text{tr}2}$ value arrived at the range of 0.09~0.16, and the materials began to fail.

The good improvements of the two-step PA treatment were discussed in the above study, and then the electrochemical corrosion behavior after different heat treatments were characterized, as shown in Figure 8. The polarization curve (Figure 8a) was obtained by taking the electrode potential as the vertical coordinate and the current as the horizontal coordinate, which represents the functional relationship between the impulse potential and the logarithm of the reaction rate current. The electrode reaction occurred during electrochemical corrosion. There was little current passed through the electrode when a reversible cell reacts. Each electrode reaction was in equilibrium. However, as the current increased to $10^{-4.8}$ A/cm², the electrode balance was destroyed and the electrode potential deviated from the equilibrium value. The irreversible degree of electrode reaction increased with the current density. The potential of the sample after the two-step + NA + BH treatment was the highest, which had a value of −1.035 v, followed by the PA + NA + BH sample (−1.055 v), and the NA + BH specimen had the lowest potential (−1.105 v). The passivation region in which the corrosion current was mild and almost kept the same appeared in all these three samples. The samples after PA treatments were not easy to be corroded, especially the two-step PA sample. In the Nyquist plots (Figure 8b), the high

frequency region of the impedance plot shows a semicircle, which is related to the redox reaction and the semicircle diameter is equal to the electron-transfer resistance. The resistance value could be estimated from the diameter of the semicircle part at higher frequencies, and decreased in the order of $R_{\text{two-step PA}} > R_{\text{PA}} > R_{\text{NA}}$. The EIS results further confirmed the results of the polarization curve.

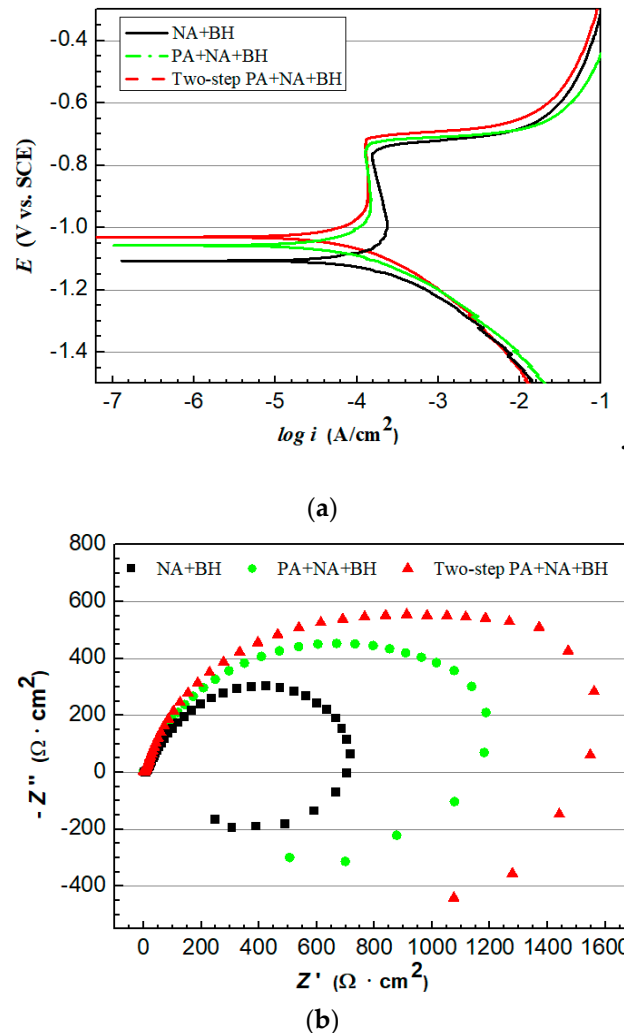


Figure 8. Electrochemical corrosion behavior after different heat treatments: (a) potentiodynamic polarization curve; (b) electrochemical impedance spectroscopy (EIS) Nyquist plots.

Figure 9 gives the 3D-MLM images of different heat treatments after the potentiodynamic polarization measurements in 3.5 wt% NaCl solution. The maximum depth of corrosion pit is decreased in the order of $D_{\text{two-step}} (33.425 \mu\text{m}) < D_{\text{PA}} (38.917 \mu\text{m}) < D_{\text{NA}} (49.484 \mu\text{m})$, which suggests that the two-step specimen has a superior corrosion resistance.

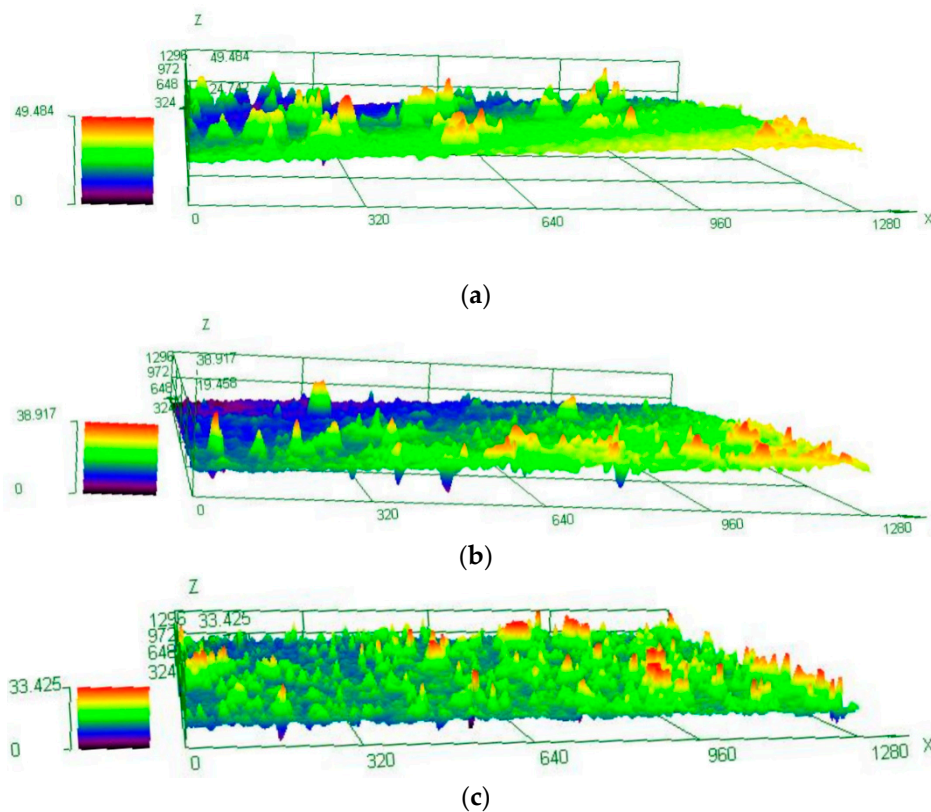


Figure 9. 3D-measuring laser microscope (MLM) images of the exposed surfaces: (a) NA + BH; (b) PA + NA + BH; (c) Two-step PA + NA + BH.

4. Conclusions

- (1) While baking at 180 °C immediately after solution treatment, the micro-hardness increased sharply first and reached the peak value (194 HV) after 10 h holding, which was a percentage improvement of 110.87% compared to the hardness under the solution condition, then had a decreasing trend and tended to become steady after 60 h.
- (2) The PA treatments decreased NA adverse effect. The main strengthening phases were GP zones before BH treatment, whereas η' were the dominant hardening phases after BH treatment. The specimen after PA under 120 °C/20 min had the lowest NA adverse effect and optimal BH response.
- (3) A novel two-step PA treatment, which further decreases the NA effect and increases the BH response compared to the optimal PA treatment, was designed. The BH value after two-step PA + NA treatment reached 168 MPa and was 21.7% higher than that of optimal PA + NA treatment. The characterizations of potentiodynamic polarization curves, EIS Nyquist plots, and 3D-MLM images showed its optimal corrosion resistance.

Author Contributions: H.L. designed the experiments and analyzed the mechanical properties data. X.-T.L. performed the TEM measurements and analyzed the mathematical model. J.-Y.W. analyzed the corrosion data. All authors contributed to the interpretation of the results and the writing of the manuscript.

Funding: The work was financially supported by National Key Research and Development Program of China (Grant No. 2016YFB0300802), a project of Shandong Province Higher Educational Science and Technology Program (Grant No. J18KA028), Key Research and Development Plan of Shandong Province (Grant No. 2019GGX102025).

Acknowledgments: Hui Li acknowledges financial support from project of Shandong Province Higher Educational Science and Technology Program (Grant No. J18KA028) and Key Research and Development Plan of Shandong Province (Grant No. 2019GGX102025). Jia-Yi Wang acknowledges financial support of National Key Research and Development Program of China (Grant No. 2016YFB0300802).

Conflicts of Interest: The authors declare no conflict of interest.

References

1. Tucker, R. Trends in automotive lightweighting. *Met. Finish.* **2013**, *111*, 23–25. [[CrossRef](#)]
2. Miller, W.S.; Zhuang, L.; Bottema, J.; Vieregge, A. Recent development in aluminum alloys for the automotive industry. *Mater. Sci. Eng. A* **2000**, *280*, 37–49. [[CrossRef](#)]
3. Hirsch, J. Recent development in aluminum for automotive applications. *Trans. Nonferr. Metal. Soc.* **2014**, *24*, 1995–2002. [[CrossRef](#)]
4. Henriksson, F.; Johansen, K. On material substitution in automotive BIWs—from steel to aluminum body sides. *Procedia CIRP* **2016**, *50*, 683–688. [[CrossRef](#)]
5. Hall, J.N.; Fekete, J.R. Steels for auto bodies: A general overview. In *Automotive Steels*; Woodhead Publishing: Cambridge, UK, 2007; pp. 19–45.
6. Santos, J.; Gouveia, R.M.; Silva, F.J.G. Designing a new sustainable approach to the change for lightweight materials in structural components used in truck industry. *J. Clean. Prod.* **2017**, *164*, 115–123. [[CrossRef](#)]
7. Ding, L.P.; He, Y.; Wen, Z.; Zhao, P.Z.; Jia, Z.H.; Liu, Q. Optimization of the pre-aging treatment for an AA6022 alloy at various temperatures and holding times. *J. Alloy. Comp.* **2015**, *647*, 238–244. [[CrossRef](#)]
8. Birol, Y. Pre-aging to improve bake hardening in a twin-roll cast Al-Mg-Si alloy. *Mater. Sci. Eng. A* **2005**, *391*, 175–180. [[CrossRef](#)]
9. Hou, W.R.; Ji, W.B.; Zhang, Z.H.; Cheng, X. The effect of homogenization temperature on the corrosion resistance of extruded 7050 Al-alloy bars. *J. Mater. Process. Technol.* **2014**, *214*, 635–640. [[CrossRef](#)]
10. Cong, F.G.; Zhao, G.; Jiang, F.; Tian, N.; Li, R. Effect of homogenization treatment on microstructure and mechanical properties of DC cast 7X50 aluminum alloy. *Trans. Nonferr. Metal. Soc.* **2015**, *25*, 1027–1034. [[CrossRef](#)]
11. Jiang, F.L.; Zurob, H.S.; Purdy, G.R.; Zhang, H. Characterizing precipitate evolution of an Al-Zn-Mg-Cu based commercial alloy during artificial aging and non-isothermal heat treatments by in situ electrical resistivity monitoring. *Mater. Charact.* **2016**, *117*, 47–56. [[CrossRef](#)]
12. Guo, W.; Guo, J.Y.; Wang, J.D.; Yang, M.; Li, H.; Wen, X.Y.; Zhang, J.W. Evolution of precipitate microstructure during stress aging of an Al-Zn-Mg-Cu alloy. *Mater. Sci. Eng. A* **2015**, *634*, 167–175. [[CrossRef](#)]
13. Liu, Y.; Jiang, D.M.; Li, W.J. The effect of multistage ageing on microstructure and mechanical properties of 7050 alloy. *J. Alloy. Compd.* **2016**, *671*, 408–418. [[CrossRef](#)]
14. Ozer, G.; Karaaslan, A. Properties of AA7075 aluminum alloy in aging and retrogression and reaging process. *Trans. Nonferr. Metal. Soc.* **2017**, *27*, 2357–2362. [[CrossRef](#)]
15. Kumar, M.; Ross, N.G. Influence of temper on the performance of a high-strength Al-Zn-Mg alloy sheet in the warm forming processing chain. *J. Mater. Process. Technol.* **2016**, *231*, 189–198. [[CrossRef](#)]
16. Huo, W.T.; Hou, L.G.; Zhang, Y.S.; Zhang, J.S. Warm formability and post-forming microstructure/property of high-strength AA7075-T6 Al alloy. *Mater. Sci. Eng. A* **2016**, *675*, 44–54. [[CrossRef](#)]
17. Cao, C.; Zhang, D.; Zhuang, L.Z.; Zhang, J.S. Improved age-hardening response and altered precipitation behavior of Al-5.2Mg-0.45Cu-2.0Zn alloy with pre-aging treatment. *J. Alloy. Compd.* **2017**, *691*, 40–43.
18. Lee, Y.S.; Koh, D.H.; Kim, H.W.; Ahn, Y.S. Improved bake-hardening response of Al-Zn-Mg-Cu alloy through pre-aging treatment. *Scr. Mater.* **2018**, *147*, 45–49. [[CrossRef](#)]
19. Marlaud, T.; Deschamps, A.; Bley, F.; Lefebvre, W.; Baroux, B. Evolution of precipitate microstructures during the retrogression and re-aging heat treatment of an Al-Zn-Mg-Cu alloy. *Acta Mater.* **2010**, *58*, 4814–4826. [[CrossRef](#)]
20. Mondolfo, L.F.; Gjostein, N.A.; Levinson, D.W. Structural changes during the aging in an Al-Mg-Zn alloy. *JOM* **1956**, *8*, 1378–1385. [[CrossRef](#)]
21. Engdahl, T.; Hansen, V.; Warren, P.J.; Stiller, K. Investigation of fine scale precipitates in Al-Zn-Mg alloys after various heat treatments. *Mater. Sci. Eng. A* **2002**, *327*, 59–64. [[CrossRef](#)]
22. Graf, R. An X-Ray study of the precipitation phenomenon in an Al-Zn-Mg alloy containing 7% Zn and 3% Mg. *Compt. Rend* **1956**, *242*, 1311–1316.

23. Ghiaasiaan, R.; Amirkhiz, B.S.; Shankar, S. Quantitative metallography of precipitating and secondary phases after strengthening treatment of net shaped casting of Al-Zn-Mg-Cu (7000) alloys. *Mater. Sci. Eng. A* **2017**, *698*, 206–217. [[CrossRef](#)]
24. Swift, H.W. Plastic instability under plane stress. *J. Mech. Phys. Solids* **1952**, *1*, 1–18. [[CrossRef](#)]



© 2019 by the authors. Licensee MDPI, Basel, Switzerland. This article is an open access article distributed under the terms and conditions of the Creative Commons Attribution (CC BY) license (<http://creativecommons.org/licenses/by/4.0/>).